RESEARCH ARTICLE | OCTOBER 02 2023

Saturation of the anomalous Hall effect at high magnetic fields in altermagnetic RuO_2

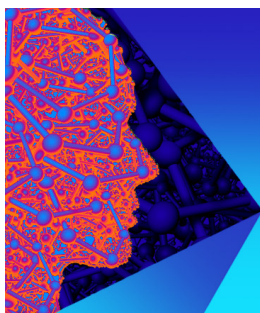**Special Collection:** Emerging Materials in Antiferromagnetic Spintronics

Teresa Tschirner ; Philipp Keßler ; Ruben Dario Gonzalez Betancourt ; Tommy Kotte ;
Dominik Kriegner ; Bernd Büchner ; Joseph Dufouleur ; Martin Kamp ; Vedran Jovic ;
Libor Smejkal; Jairo Sinova ; Ralph Claessen ; Tomas Jungwirth ; Simon Moser ;
Helena Reichlova ; Louis Veyrat ✉

Check for updates

View Online

Export Citation

CrossMark

19 March 2024 15:58:29

Saturation of the anomalous Hall effect at high magnetic fields in altermagnetic RuO$_2$

View Online   Export Citation   CrossMark

Teresa Tschirner,[1,2] (iD) Philipp Keßler,[2,3] (iD) Ruben Dario Gonzalez Betancourt,[1,4] (iD) Tommy Kotte,[5] (iD)
Dominik Kriegner,[4,6] (iD) Bernd Büchner,[1,2,6] (iD) Joseph Dufouleur,[1] (iD) Martin Kamp,[7] (iD) Vedran Jovic,[8] (iD)
Libor Smejkal,[4,9] Jairo Sinova,[4,9] (iD) Ralph Claessen,[2,3] (iD) Tomas Jungwirth,[4,10] (iD) Simon Moser,[2,3] (iD)
Helena Reichlova,[4,6] (iD) and Louis Veyrat[1,2,3,a)] (iD)

AFFILIATIONS

[1]Leibniz Institute for Solid State and Materials Research, IFW Dresden, Helmholtzstr. 20, 01069 Dresden, Germany
[2]Würzburg-Dresden Cluster of Excellence ct.qmat, Dresden, Germany
[3]Physikalisches Institut, Universität Würzburg, D-97074 Würzburg, Germany
[4]Institute of Physics ASCR, v.v.i., Cukrovarnická 10, 162 53 Prague, Czech Republic
[5]Hochfeld-Magnetlabor Dresden (HLD-EMFL), Helmholtz-Zentrum Dresden-Rossendorf, 01328 Dresden, Germany
[6]Institut für Festkörper- und Materialphysik, Technische Universität Dresden, 01069 Dresden, Germany
[7]Physikalisches Institut, Universität Würzburg, D-97074 Würzburg, Germany and Röntgen Center for Complex Material
Systems, Universität Würzburg, D-97074 Würzburg, Germany
[8]Earth Resources and Materials, Institute of Geological and Nuclear Science, Lower Hutt 5010, New Zealand and MacDiarmid
Institute for Advanced Materials and Nanotechnology, Wellington 6012, New Zealand
[9]Institut für Physik, Johannes Gutenberg Universität Mainz, 55128 Mainz, Germany
[10]School of Physics and Astronomy, University of Nottingham, NG7 2RD Nottingham, United Kingdom

Note: This paper is part of the Special Topic on Emerging Materials in Antiferromagnetic Spintronics.
[a)]Author to whom correspondence should be addressed: reichlh@fzu.cz and l.veyrat@ifw-dresden.de

ABSTRACT

Observations of the anomalous Hall effect in RuO$_2$ and MnTe have demonstrated unconventional time-reversal symmetry breaking in the electronic structure of a recently identified new class of compensated collinear magnets, dubbed altermagnets. While in MnTe, the unconventional anomalous Hall signal accompanied by a vanishing magnetization is observable at remanence, the anomalous Hall effect in RuO$_2$ is excluded by symmetry for the Néel vector pointing along the zero-field [001] easy-axis. Guided by a symmetry analysis and *ab initio* calculations, a field-induced reorientation of the Néel vector from the easy-axis toward the [110] hard-axis was used to demonstrate the anomalous Hall signal in this altermagnet. We confirm the existence of an anomalous Hall effect in our RuO$_2$ thin-film samples, whose set of magnetic and magneto-transport characteristics is consistent with the earlier report. By performing our measurements at extreme magnetic fields up to 68 T, we reach saturation of the anomalous Hall signal at a field $H_c \simeq 55$ T that was inaccessible in earlier studies but is consistent with the expected Néel-vector reorientation field.

I. INTRODUCTION

The anomalous Hall effect (AHE) is a macroscopic linear response probe of time-reversal ($\mathcal{T}$) symmetry breaking in the electronic structure of magnetic materials.[1–6] The established mechanisms include $\mathcal{T}$-symmetry breaking and AHE in conventional ferromagnets or in non-collinear magnetic structures.[1–9] Recently, these have been extended by a novel and unconventional mechanism of $\mathcal{T}$-symmetry breaking, resulting in the prediction[2,10] and subsequently observation of the AHE[11–13] in a class of compensated collinear magnets whose opposite magnetic moments reside on crystal-sublattices connected by rotation symmetries.[2,14,15] Materials of this third unconventional class of collinear magnets, complementing the conventional ferromagnetic and antiferromagnetic classes, have a characteristic alternating spin polarization in both real-space crystal structure and momentum-space electronic structure that suggests the term altermagnets.[14,15] The $\mathcal{T}$-symmetry breaking nature of the AHE thus implies that the sign of the AHE in altermagnets flips when reversing the sign of the Néel vector.[2,10]

In contrast to ferromagnets, where AHE is always allowed, AHE in altermagnets can be allowed or excluded by symmetry depending on the orientation of the Néel vector with respect to the crystal axes.[2,10] (For a comprehensive symmetry discussion of AHE in ferromagnets, altermagnets, and non-collinear magnets, we refer to recent review articles in Refs. 1 and 15.) In altermagnetic MnTe, for example, the AHE measured in the (0001) c-plane of this hexagonal crystal is allowed for by the Néel vector pointing along one of the equivalent $\langle 1\bar{1}00 \rangle$ easy axes.[11,12] As a result, Hall measurements in the (0001) c-plane show a hysteretic AHE signal of opposite sign at opposite saturating fields with a coercivity on the order of a few T when sweeping the magnetic field along the c-axis, with a finite remanent AHE at zero field.

Altermagnetic RuO$_2$ shows a qualitatively distinct AHE phenomenology.[10,11] For the Néel vector along the magnetic easy-axis, which corresponds to the [001] axis of this tetragonal rutile crystal, the AHE is excluded by symmetry.[2,10] An AHE is allowed by symmetry only when the Néel vector has a non-zero component in the (001) plane. As a result, no AHE signal is detected for a Hall bar patterned in the (001)-plane when sweeping the out-of-plane field along the [001] c-axis.[11] This sample and field geometry do not break the symmetry between opposite signs of the Néel-vector reorientation angle from the [001] easy axis.[11,16] Therefore, even if the applied field was strong enough to cause a spin-flop reorientation of the Néel vector toward the (001)-plane, it would not generate a non-zero net AHE signal odd in the applied field.[11]

In contrast, a magnetic field applied along the [110] direction induces a continuous rotation of the Néel vector by an angle α from the [001] toward the [110] axis, given approximately by $\sin \alpha \sim H/H_c$ (for $H < H_c$).[11,16] Here, the direction of the Néel vector rotation is given by the sign of the magnetic field H, and H_c quantifies the field strength that aligns the Néel vector along the out-of-plane [110] axis. The critical field H_c hereby depends on the exchange interaction, the magneto-crystalline anisotropy, and the Dzyaloshinskii-Moriya interaction (DMI) in terms of the thermodynamic potential,[16] and in rutiles, it tends to be generally weaker than the spin-flop reorientation field applied along the [001] easy axis. In RuO$_2$, H_c was estimated to be above 50 T, i.e., beyond the field available in the earlier AHE study[11] but below the [001] spin-flop field, whose strength was estimated to exceed 100 T.[11]

In the recent study,[11] a non-linear Hall signal at high fields in RuO$_2$ Hall bars patterned in the (110)-plane was interpreted as a strong, yet unsaturated, AHE generated by the reorientation of the Néel vector into the (1$\bar{1}$0)-plane by the applied [110] field. The opposite direction of the Néel vector rotation for opposite applied fields gave the opposite sign of the AHE.[11] The detected AHE signal was, therefore, odd in the applied [110]-field and vanished at zero field. A comparison to the measurements in the (001)-plane Hall bars evidenced a strong AHE contribution in the (110)-plane samples, dominating the ordinary Hall contribution over the whole field range up to 50 T.[11] However, as H_c exceeded the experimentally available magnetic field range, no saturation of the AHE has been observed. The appearance of a saturation would make a strong case for an AHE generated by the Néel vector reorientation, for which such a saturation above H_c is expected.

In this study, we present magnetotransport measurements on (110)-plane oriented RuO$_2$ samples analogous to those explored in Ref. 11. We further optimized the film preparation protocol to achieve high crystalline quality and stoichiometry, as evidenced by a thorough structural characterization. We performed on these samples a systematic magnetic and magneto-transport characterization up to magnetic fields of 68 T. Our results demonstrate consistency with Ref. 11 below 50 T, and by going beyond 50 T, magnetic fields allow us to reach saturation of the AHE signal. The observation of saturation completes the experimental evidence of the AHE in this workhorse altermagnet.[10,11,17–19]

II. THIN FILM GROWTH AND CHARACTERISATION

Our RuO$_2$(110) samples were grown epitaxially on (110)-oriented substrates of rutile TiO$_2$ (CRYSTAL GmbH) using a commercial pulsed laser deposition (PLD) setup (TSST B.V.) with a pulsed excimer laser (COMPex Pro 205/KrF, 248 nm). Prior to growth, the substrates were cleaned in subsequent ultrasonic baths of isopropanol and acetone (20 min, puriss.) and annealed for 5 h in a tube furnace at 820 °C with an oxygen flow of 20 l/h to obtain a stepped-terrace morphology. The PLD growth conditions were set to an oxygen partial pressure of 1×10^{-3} mbar and a substrate temperature of 700 K (two-color pyrometer, IMPAC). Then, the sintered RuO$_2$ powder target (TOSHIMA Manufacturing Co., Ltd.) was ablated by 32.000 laser pulses at a repetition rate of 10 Hz. The laser energy density was gradually increased from 0.7 to 1.4 J/cm^2 to compensate for laser induced oxygen deficiencies and a consequent increase in target reflectivity during deposition. The film growth was monitored by reflective high-energy electron diffraction (RHEED, STAIB) and post-characterized by x-ray reflectivity (XRR) and x-ray diffraction (XRD) on a Rigaku SmartLab rotating anode with parabolic mirror and Ge channel cut monochromator using 8047.8 eV Cu Kα radiation, as well as x-ray photoelectron spectroscopy (XPS, OMICRON, 1486.6 eV Al Kα; data not shown) to check the stoichiometry.

The film characterization results are shown in Fig. 1. Figure 1(a) shows an XRD close-up around the 110 Bragg peak of the TiO$_2$ substrate and the epitaxial RuO$_2$ thin film, taken from the full range scan in the inset, and providing lattice parameters that are in excellent agreement with the literature values.[11] The data are further compared to simulations for a 9.8 nm thick film with 0.5 nm roughness,
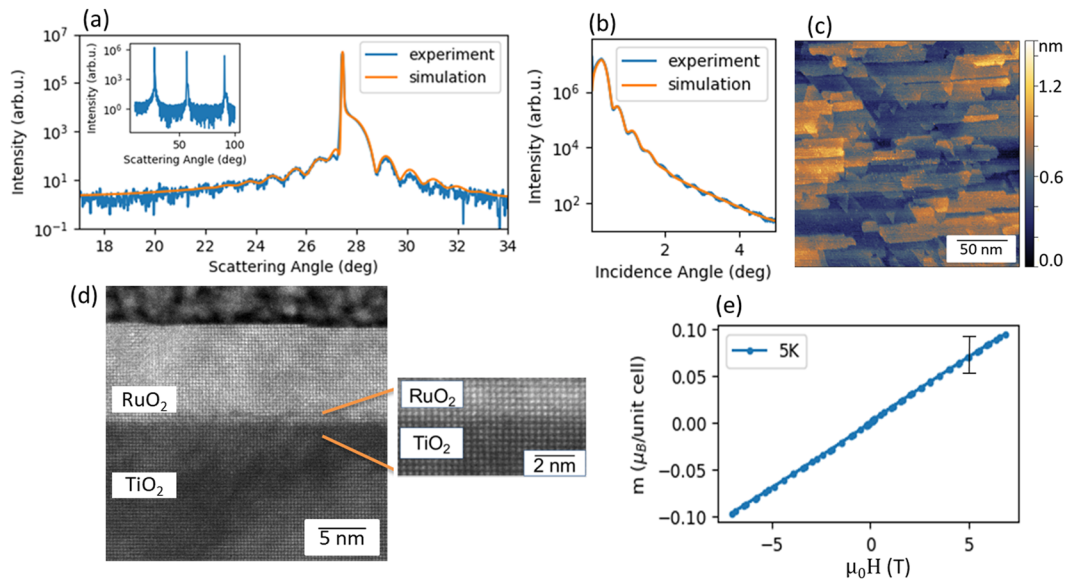
FIG. 1. Growth and characterization of RuO_2 thin film on a TiO_2(110). (a) XRD data of the 110 Bragg peak (full range in the inset) and (b) XRR show good agreement with simulations for a 9.8 nm thick film with 0.5 nm roughness. (c) STM shows a smooth film surface. (d) TEM shows epitaxial and dislocation-free growth of RuO_2(110) on TiO_2(110). (e) SQUID magnetometery measurements on the RuO_2/TiO_2 sample with subtracted background based on a TiO_2 reference measurement. The large error bar in the magnetization data is due to the weak field-induced magnetic moments in RuO_2.

obtained via the Parrat formalism and a dynamic diffraction model as implemented in Ref. 20.

The XRR in Fig. 1(b) confirms the thickness of our sample to be $\approx 9 - 10$ nm. Both XRR and XRD show thickness fringes corresponding to the same thickness, proving excellent crystalline quality with a coherent crystal lattice from the interface with the substrate to the surface and correspondingly low roughness. The crystalline quality is further confirmed by "scanning transmission electron microscopy (STEM, FEI Titan 80–300, U = 300 kV, I = 120 pA) in Fig. 1(d).

The low roughness suggested by XRD and XRR is consistently demonstrated by scanning tunneling microscopy (STM) images (Omicron VT-STM, constant current mode, RT, U = 500 mV, I = 0.05 nA) in Fig. 1(c), yielding a rms of <2 nm.

A superconducting quantum interference device (SQUID) MPMS3 magnetometry measurement of our sample at 5 K is shown in Fig. 1(e). A measurement on a bare TiO_2 substrate is used as a reference to subtract the background from the data measured on the 9 nm RuO_2 film. As the signal from the magnetic RuO_2 moments is extremely small as compared to the TiO_2 background, the presented magnetometry data are subject to a large error bar. However, the weak field-induced moment is consistent with the previous report by Feng *et al.*[11]
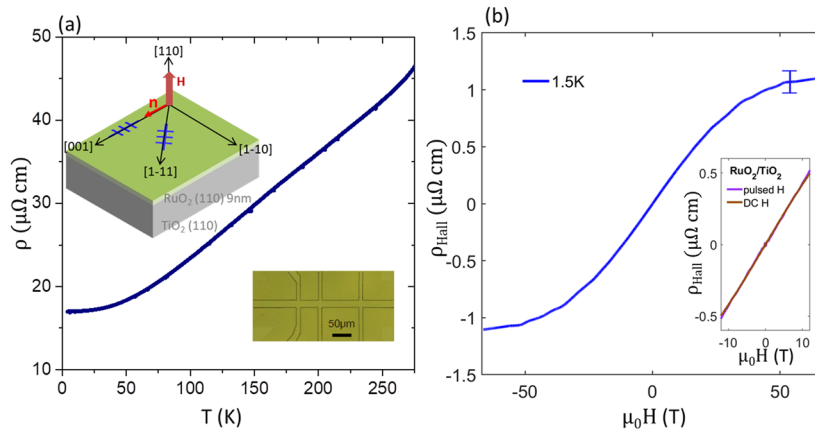
III. MAGNETO-TRANSPORT

To perform transport measurements, Hall bars were fabricated by e-beam lithography out of the RuO_2 thin films. Trenches defining the Hall bars were etched by argon ion beam etching. The Hall bars have different orientations in the sample (110) plane, either along the [001] or the [1$\bar{1}$1] axes, as shown in the inset of Fig. 2(a). All

Hall bars have a width of 10 μm, with distances between contacts of 50 and 100 μm, as shown in the second inset of Fig. 2(a).

The magneto-transport measurements were first performed in a static magnetic field in a standard Quantum Design Physical Properties Measurement System (QD PPMS) setup, and afterward, the same device was studied in the high magnetic field laboratory (HLD) in Dresden-Rossendorf using pulsed magnetic fields up to 68 T with pulses of 100 ms duration and a rise time of 35 ms. The magnetic field was applied in the out-of-plane sample direction, which corresponds to the RuO_2 [110] crystalline direction. To investigate the angular dependence of the Hall resistivity, the magnetic field was additionally tilted by $\theta = \pm 45°$ toward [001], as illustrated in the inset of Fig. 4. An alternating current (AC) with an amplitude of 5 μA was applied, and the voltage was measured using a numerical lock-in technique with frequencies in the kHz range to suppress the noise level and spurious effects from the pulsed magnetic field. The presented high magnetic field data were measured on two samples grown under the same conditions, showing reproducible results.

Figure 2(a) shows the temperature dependent longitudinal resistivity ρ, which decreases with decreasing temperature, indicating metallic behavior in the thin films. The main result of our study is the Hall resistivity ρ_{Hall} measured up to 68 T, which is shown in Fig. 2(b). The measurement in pulsed magnetic fields results in higher noise levels; therefore, the curve was smoothed using a Savitzky–Golay filter, and the noise is indicated by the error bar. The Hall resistivity shows a pronounced non-linearity, exhibiting a non-zero curvature beyond 20 T. This is consistent with the measurements on RuO_2(110) films reported in Ref. 11. However, with the maximum accessible magnetic field of 50 T, a clear signature

FIG. 2. Magneto-transport in (110)-oriented RuO$_2$ thin films. (a) Temperature dependence of the longitudinal resistivity showing metallic behavior. Upper inset: Orientation of the Hall bars with respect to the crystal directions and the directions of the Néel-vector easy axis (**n**) and applied field axis (**H**). Lower inset: optical microscopy image of the RuO$_2$ Hall bar, highlighted by dashed lines. (b) Antisymmetrized transverse resistivity (Hall resistivity) of a RuO$_2$ Hall bar oriented in the [001] direction measured in the high magnetic field facility up to 68 T. The inset compares the pulsed field to the in-house static field measurements up to 12 T.

of the saturation of the AHE signal was not observed in Ref. 11. In our data in Fig. 2(b), we observe the saturation of the AHE above $H_c \simeq 55$ T. This field range is consistent with the expected 50–100 T scale of the reorientation field of the Néel vector from the [001] easy axis to the [110] hard axis.[11] Moreover, the very weak asymptotic slope above H_c (corresponding to the ordinary Hall effect), together with the overall magnitude of ρ_{Hall}, shows that the AHE signal dominates over the ordinary Hall contribution over the entire range of applied magnetic fields.

Temperature-dependent magneto-transport data are shown in Fig. 3. The longitudinal magnetoresistance in Fig. 3(a) reaches 15% at 68 T and low temperature. At low fields, the magnetoresistance is roughly parabolic, and the amplitude of the magnetoresistance strongly decreases with increasing temperature. The

temperature-dependent Hall resistivity is shown in Fig. 3(b). The overall ρ_{Hall} amplitude decreases with increasing temperature, up to our maximum temperature of 200 K. In addition, we see a clear saturation of the Hall signal at temperatures up to 80 K.

Figure 3(c) highlights the decrease in the Hall resistivity at 68 T with increasing temperature for two Hall bars patterned along the [001] and [1$\bar{1}$1] directions. The data of both samples are in remarkable agreement, indicating the Néel vector in both cases to be rotated into the (1$\bar{1}$0) plane upon application of the [110] oriented magnetic field, as illustrated in the inset of Fig. 2(a).

To further investigate the influence of a magnetic field component applied along the [001] easy axis on the AHE, we measure the Hall resistivity while tilting the field away from the [110] direction toward the [001] direction. The results are presented in Fig. 4,
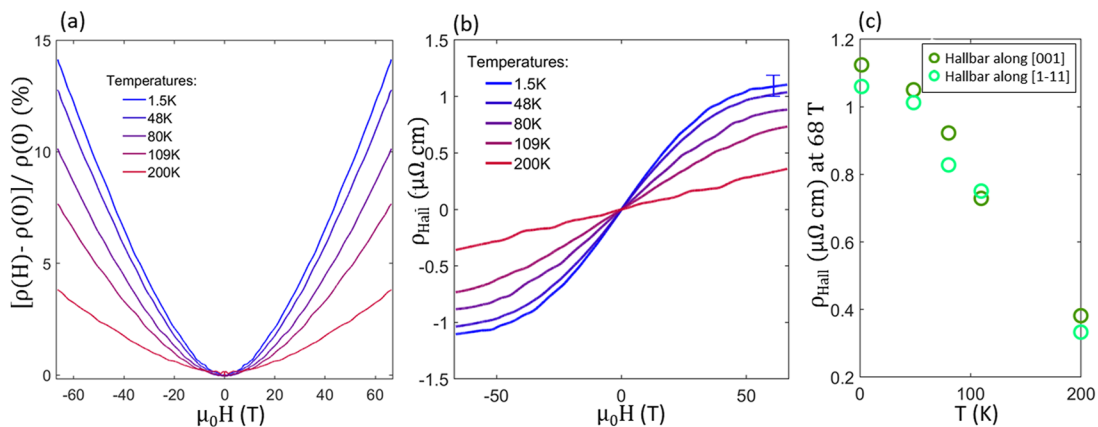
FIG. 3. Temperature dependent magneto-transport data of RuO$_2$(110). (a) Temperature dependence of the symmetrized longitudinal magnetoresistance and (b) the antisymmetrized transverse resistivity (Hall resistivity). The error bar indicates the uncertainties caused by noise in high magnetic fields. (c) Comparison of the temperature dependencies of the Hall resistivity at B = 68 T for Hall bars oriented along the [001] and [1$\bar{1}$1] directions, respectively.
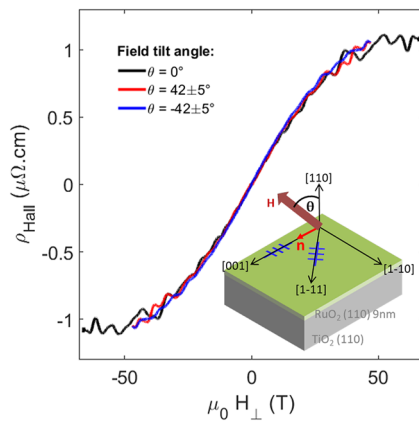
FIG. 4. Effect of magnetic field tilting on the Hall resistivity in RuO$_2$(110). The Hall resistivity is shown with respect to the out-of-plane component of the tilted magnetic field. The magnetic field was rotated by $\pm 45°$ toward the [001] axis. The inset shows the orientation of the Hall bars with respect to the crystal directions of the Néel-vector easy axis (**n**) and the applied field axis (**H**) rotated at an angle θ.

showing the Hall resistivity as a function of the [110] field component $H_{\perp}$ for tilt angles of $\theta = \pm 45°$. Again, all datasets are in remarkable agreement, confirming that the AHE solely depends on the projection of the field onto the [110] axis. Most importantly, this implies that applying a magnetic field along the easy [001] axis does not tilt the Néel vector into the (110) plane, as this would result in saturation at lower fields.

IV. CONCLUSION

In conclusion, we have systematically investigated the structural, magnetic, and magneto-transport characteristics of epitaxial thin-film RuO$_2$(110) grown on TiO$_2$(110) substrates. The excellent crystalline quality of our films is demonstrated by XRR, TEM, and STM measurements. Our magnetotransport results below 50 T are qualitatively consistent with the earlier report in Ref. 11 and provide additional confirmation of the unconventional AHE originating from collinearly compensated magnetic order in altermagnetic RuO$_2$.

Going beyond a mere confirmation, our work augments the range of accessible magnetic fields up to 68 T, fields that are large enough to saturate the AHE resistivity. The corresponding saturation field is consistent with earlier estimates.[11]

AUTHOR DECLARATIONS

Conflict of Interest

The authors have no conflicts to disclose.

Author Contributions

Teresa Tschirner: Conceptualization (equal); Data curation (equal); Formal analysis (equal); Investigation (equal); Methodology (equal); Visualization (equal); Writing – original draft (equal). **Philipp Kesler**: Conceptualization (equal); Data curation (equal); Formal analysis (equal); Investigation (equal); Methodology (equal); Resources (equal); Visualization (equal); Writing – original draft (equal). **Ruben Dario Gonzalez Betancourt**: Data curation (equal); Formal analysis (equal); Investigation (equal); Methodology (equal); Visualization (equal). **Tommy Kotte**: Conceptualization (equal); Data curation (equal); Formal analysis (equal); Investigation (equal); Methodology (equal). **Dominik Kriegner**: Data curation (equal); Formal analysis (equal); Visualization (equal). **Bernd Büchner**: Conceptualization (equal); Formal analysis (equal); Funding acquisition (equal); Project administration (equal); Resources (equal); Supervision (equal); Validation (equal). **Joseph Dufouleur**: Conceptualization (equal); Data curation (equal); Formal analysis (equal); Investigation (equal); Methodology (equal); Supervision (equal). **Martin Kamp**: Data curation (equal); Investigation (equal); Resources (equal); Validation (equal); Visualization (equal). **Vedran Jovic**: Data curation (equal); Formal analysis (equal); Methodology (equal); Resources (equal); Validation (equal); Visualization (equal). **Libor Smejkal**: Conceptualization (equal); Formal analysis (equal); Investigation (equal); Validation (equal). **Jairo Sinova**: Conceptualization (equal); Funding acquisition (equal); Methodology (equal); Supervision (equal); Validation (equal). **Ralph Claessen**: Conceptualization (equal); Funding acquisition (equal); Investigation (equal); Project administration (equal); Supervision (equal). **Tomas Jungwirth**: Conceptualization (equal); Formal analysis (equal); Funding acquisition (equal); Methodology (equal); Supervision (equal); Writing – original draft (equal). **Simon Moser**: Data curation (equal); Investigation (equal); Methodology (equal); Project administration (equal); Resources (equal); Supervision (equal). **Helena Reichlova**: Data curation (equal); Formal analysis (equal); Methodology (equal); Supervision (equal); Validation (equal); Visualization (equal); Writing – original draft (equal). **Louis Veyrat**: Conceptualization (equal); Data curation (equal); Formal analysis (equal); Funding acquisition (equal); Methodology (equal); Project administration (equal); Supervision (equal); Writing – original draft (equal).

DATA AVAILABILITY

The data that support the findings of this study are available from the corresponding author upon reasonable request.

19 March 2024 15:58:29

REFERENCES

[1] N. Nagaosa, J. Sinova, S. Onoda, A. H. MacDonald, and N. P. Ong, "Anomalous Hall effect," Rev. Mod. Phys. **82**, 1539 (2010); arXiv:0904.4154.

[2] L. Šmejkal, A. H. MacDonald, J. Sinova, S. Nakatsuji, and T. Jungwirth, "Anomalous Hall antiferromagnets," Nat. Rev. Mater. **7**, 482 (2022); arXiv:2107.03321.

[3] R. Shindou and N. Nagaosa, "Orbital ferromagnetism and anomalous Hall effect in antiferromagnets on the distorted fcc lattice," Phys. Rev. Lett. **87**, 116801 (2001); arXiv:0108322[cond-mat].

[4] Y. Machida, S. Nakatsuji, S. Onoda, T. Tayama, and T. Sakakibara, "Time-reversal symmetry breaking and spontaneous Hall effect without magnetic dipole order," Nature **463**, 210 (2010).

[5] H. Chen, Q. Niu, and A. H. Macdonald, "Anomalous hall effect arising from noncollinear antiferromagnetism," Phys. Rev. Lett. **112**, 017205 (2014); arXiv:1309.4041.

[6] J. Kübler and C. Felser, "Non-collinear antiferromagnets and the anomalous Hall effect," Europhys. Lett. **108**, 67001 (2014); arXiv:1410.5985.

[7] S. Nakatsuji, N. Kiyohara, and T. Higo, "Large anomalous Hall effect in a non-collinear antiferromagnet at room temperature," Nature **527**, 212 (2015).

[8] N. Kiyohara, T. Tomita, and S. Nakatsuji, "Giant anomalous hall effect in the chiral antiferromagnet Mn_3Ge," Phys. Rev. Appl. **5**, 064009 (2016).

[9] A. K. Nayak, J. E. Fischer, Y. Sun, B. Yan, J. Karel, A. C. Komarek, C. Shekhar, N. Kumar, W. Schnelle, J. Kübler, C. Felser, and S. S. Parkin, "Large anomalous Hall effect driven by a nonvanishing Berry curvature in the noncollinear antiferromagnet Mn_3Ge," Sci. Adv. **2**, e1501870 (2016); arXiv:1511.03128.

[10] L. Šmejkal, R. González-Hernández, T. Jungwirth, and J. Sinova, "Crystal time-reversal symmetry breaking and spontaneous Hall effect in collinear antiferromagnets," Sci. Adv. **6**, eaaz8809 (2020); arXiv:1901.00445.

[11] Z. Feng, X. Zhou, L. Šmejkal, L. Wu, Z. Zhu, H. Guo, R. González-Hernández, X. Wang, H. Yan, P. Qin, X. Zhang, H. Wu, H. Chen, Z. Meng, L. Liu, Z. Xia, J. Sinova, T. Jungwirth, and Z. Liu, "An anomalous Hall effect in altermagnetic ruthenium dioxide," Nat. Electron. **5**, 735 (2022).

[12] R. D. Gonzalez Betancourt, J. Zubáč, R. Gonzalez-Hernandez, K. Geishendorf, Z. Šobáň, G. Springholz, K. Olejník, L. Šmejkal, J. Sinova, T. Jungwirth, S. T. B. Goennenwein, A. Thomas, H. Reichlová, J. Železný, and D. Kriegner, "Spontaneous anomalous Hall effect arising from an unconventional compensated magnetic phase in a semiconductor," Phys. Rev. Lett. **130**, 036702 (2023); arXiv:2112.06805.

[13] K. Samanta, M. Ležaić, M. Merte, F. Freimuth, S. Blügel, and Y. Mokrousov, "Crystal Hall and crystal magneto-optical effect in thin films of $SrRuO_3$," J. Appl. Phys. **127**, 213904 (2020).

[14] L. Šmejkal, J. Sinova, and T. Jungwirth, "Beyond conventional ferromagnetism and antiferromagnetism: A phase with nonrelativistic spin and crystal rotation symmetry," Phys. Rev. X **12**, 031042 (2022).

[15] L. Šmejkal, J. Sinova, and T. Jungwirth, "Emerging research landscape of altermagnetism," Phys. Rev. X **12**, 040501 (2022); arXiv:2204.10844.

[16] A. N. Bazhan and C. Bazan, "Weak ferromagnetism in CoF_2 and NiF_2," Sov. Phys. JETP **42**, 898 (1976).

[17] A. Bose, N. J. Schreiber, R. Jain, D.-f. Shao, H. P. Nair, J. Sun, X. S. Zhang, D. A. Muller, E. Y. Tsymbal, D. G. Schlom, and D. C. Ralph, "Tilted spin current generated by an antiferromagnet," Nat. Electron. **5**, 263 (2022); arXiv:2108.09150.

[18] H. Bai, L. Han, X. Y. Feng, Y. J. Zhou, R. X. Su, Q. Wang, L. Y. Liao, W. X. Zhu, X. Z. Chen, F. Pan, X. L. Fan, and C. Song, "Observation of spin splitting torque in a collinear antiferromagnet RuO_2," Phys. Rev. Lett. **128**, 197202 (2022); arXiv:2109.05933.

[19] S. Karube, T. Tanaka, D. Sugawara, N. Kadoguchi, M. Kohda, and J. Nitta, "Observation of spin-splitter torque in collinear antiferromagnetic RuO_2," Phys. Rev. Lett. **129**, 137201 (2022); arXiv:2111.07487.

[20] D. Kriegner, E. Wintersberger, and J. Stangl, "*xrayutilities*: a versatile tool for reciprocal space conversion of scattering data recorded with linear and area detectors," J. Appl. Crystallogr. **46**, 1162 (2013).